Int. J. Electrochem. Sci., 10 **(2015)** 9359 - 9369

International Journal of
ELECTROCHEMICAL
SCIENCE
www.electrochemsci.org

Effects of Heat Treatment on Microstructure and Pitting Corrosion Resistance of 2205 Duplex Stainless Steel

Xiangyong Liu[2], *Kada Xia*[1], *Junchao Niu, Zhen Xiang*[1], *Biao Yan*[1], *Wei Lu*[1,*]

[1] School of Materials Science and Engineering, Shanghai Key Lab. of D&A for Metal-Functional Materials, Tongji University, Shanghai 200092, China
[2] Ji'nan Rail Transit Group Co. Ltd., No.2000 Shunhua Rd., Jinan 250101, China
[*]E-mail: weilu@tongji.edu.cn

Received: 28 July 2015 / *Accepted:* 27 August 2015 / *Published:* 30 September 2015

In this study, the effect of heat treatment processes on microstructure and pitting corrosion resistance of 2205 duplex stainless steel within the temperature range of 500℃~650℃ was investigated. According to TEM analysis, intermediate phase and R phase begin to precipitate after aging 48h at 590 ℃ and σ phase begins to precipitate after aging 5h at 650 ℃. The anodic polarization results show that the pitting resistance of samples was reduced both at aging temperatures of 590℃ and 650℃. The results also indicate that the precipitation of intermediate phase obviously decreased the pitting corrosion resistance of 2205 duplex stainless steel. In addition, it was observed that the pits inclined to nucleate and grow near the precipitations in the ferrite and α/γ interface boundary.

Keywords: 2205 Duplex stainless steel, Heat treatment, Intermediate phase, Pitting

1. INTRODUCTION

2205 duplex stainless steel(DSS) which has a two phase microstructure: austenite and delta ferrite, possesses good resistance to pitting and corrosion cracking. Owing to the excellent properties, such as high strength, good corrosion resistance, duplex stainless steel has a large amount of applications in aggressive marine environments [1-6]. However, the corrosion resistance is always the essential problem that limits the more wide use of duplex stainless steel [7,8].

The presence of considerable amount of elements, like Cr, Ni, Mo, M, N, gives 2205 duplex stainless steel excellent resistance in chloride containing solutions. Nevertheless, during heating within the temperature range of 500℃~650℃, the intermediate phase was precipitated, including carbides, π phases, sigma phases and R phases [9-14]. Sigma phase is precipitated at temperature of 600℃ to 1000℃. On the one hand, it has been reported that sigma phase is the most adversely intermediate

phase which can reduce the toughness [15]. On the other hand, sigma phase is mainly made up of Cr. The precipitation or dissolution of this phase can reduce the number of Cr in the area so that the pitting corrosion resistance of duplex stainless steel will be decreased [10, 16-17]. According to the literatures [11-13], the R phase is formed much earlier than the sigma phase during the temperature range of 550℃~750℃. The R phase is rich in Mo. Therefore, the precipitation of R phase results in the reduction of Mo and the pitting corrosion resistance.

Therefore, the aim of this work is to determine the effect of heat treatments between 500℃~650℃on the microstructure and pitting corrosion resistance. The microstructure was studied by optical microscopy (OM), scanning electron microscopy (SEM) and transmission electron microscopy (TEM). The pitting corrosion resistance was performed by electrochemical measurements in 3.5 wt.% NaCl solution. The relationship between the microstructure and the electrochemical tests was disscussed.

2. EXPERIMENTAL

Table 1. Nominal chemical composition of 2205 duplex stainless steel

Element	C	Mn	Si	S	P	Ni	Cr	Mo	N	Fe
Wt.%	0.023	1.35	0.38	0.001	0.026	4.83	22.07	2,37	0.19	Bal.

The used materials was commercial 2205 duplex stainless steel with the composition shown in Table 1. Samples with a certain size were cut directly from the 2205 duplex stainless steel bars. The samples were solution treated at 1050℃ for 30min in the high temperature box type resistance furnace and quenched in water. Then the experimental samples were aged at 590℃ for 10,24,48,72 and 96h, and at 650℃ for 2,5,10, 18 and 24h.

X-ray diffraction(XRD) analysis of the experimental samples were investigated using a X-Ray diffractometer with CuKα radiation. The microstructure of the processed samples was observed by OM, field emission SEM and TEM. The samples for TEM experiment were firstly ground to a thickness of about 0.6 mm, and then were mechanically polished to a thickness of about 25um. Finally the samples were reducing via a twin-jet machine and a ion beam thinner.

The samples used for electrochemical measurements were all cut into a cube shape with a length of 1cm. First of all, the samples were ground successively in turns with 220-, 400-, 600-, 800-, and 1000- SiC papers, mechanically polished, and cleaned with deionized water to get a fine surface. Prior to the test, high purity N_2 were filled into the solution no less than 30min to remove the oxygen which was dissolved in the solution. The pitting tests were determined by anodic polarisation curves in a 500ml 3.5%NaCl solution at 20℃, starting from the corrosion potential and with a scan rate of 9 mV/min. Metallographic observation of the pits which were generated by potentiostatic measurements in a 3.5%NaCl solution were analysed by OM and SEM.

3. RESULTS AND DISCUSSION

3.1. Microstructures and precipitates

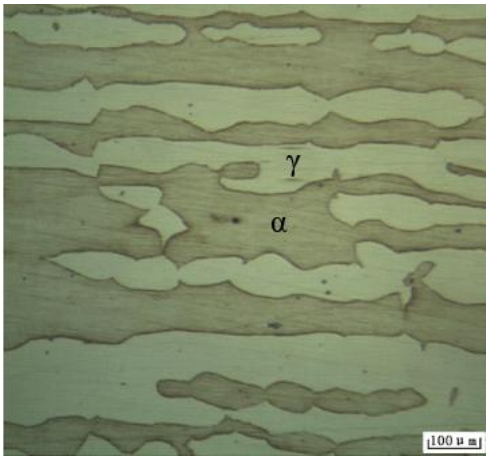

Figure 1. Optical microstructure of 2205 DSS after solution treatment at 1050℃ for 30min

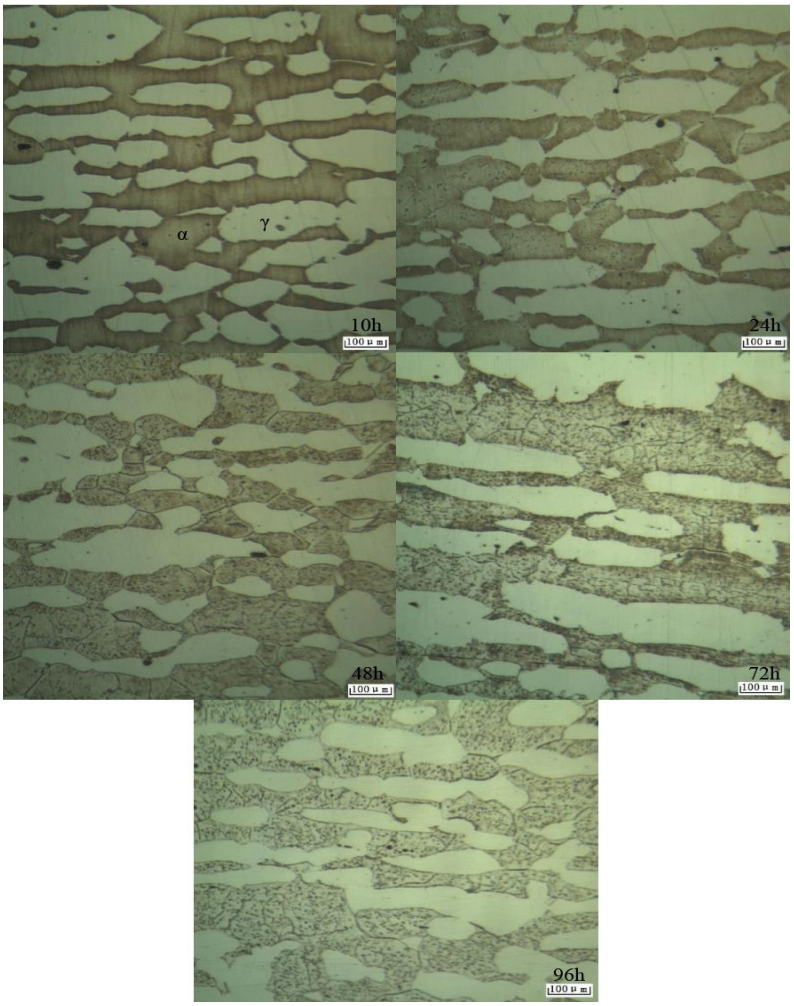

Figure 2. Optical microstructure of 2205 DSS aged at aging temperature of 590℃ for different aging time (10, 24, 48, 72, and 96h)

Fig. 1 shows the microstructure of the 2205 duplex stainless steel after solution at 1050℃ for 30min. The bright part is the austenite phase(γ), the dark part representing the ferrite phase(α). This figure suggests that the bar-like austenite phase is embedded in the ferrite matrix, and the volume fraction of the austenite is close to that of the ferrite, indicating a good balance of both phases.

Fig.2 shows the microstructures of samples aged at 590℃ for different time (10, 24, 48, 72, and 96h). As can be observed, the microstructure of 2205 DSS treated for 10h has no significant change compared with Fig.1. With the increasing aging time (from 24h to 96h), black grains appear in the α phase, and the amount of the black grains increases, except that there is no change in the grain size. Subsequently, the volume fraction of α phase decreases.

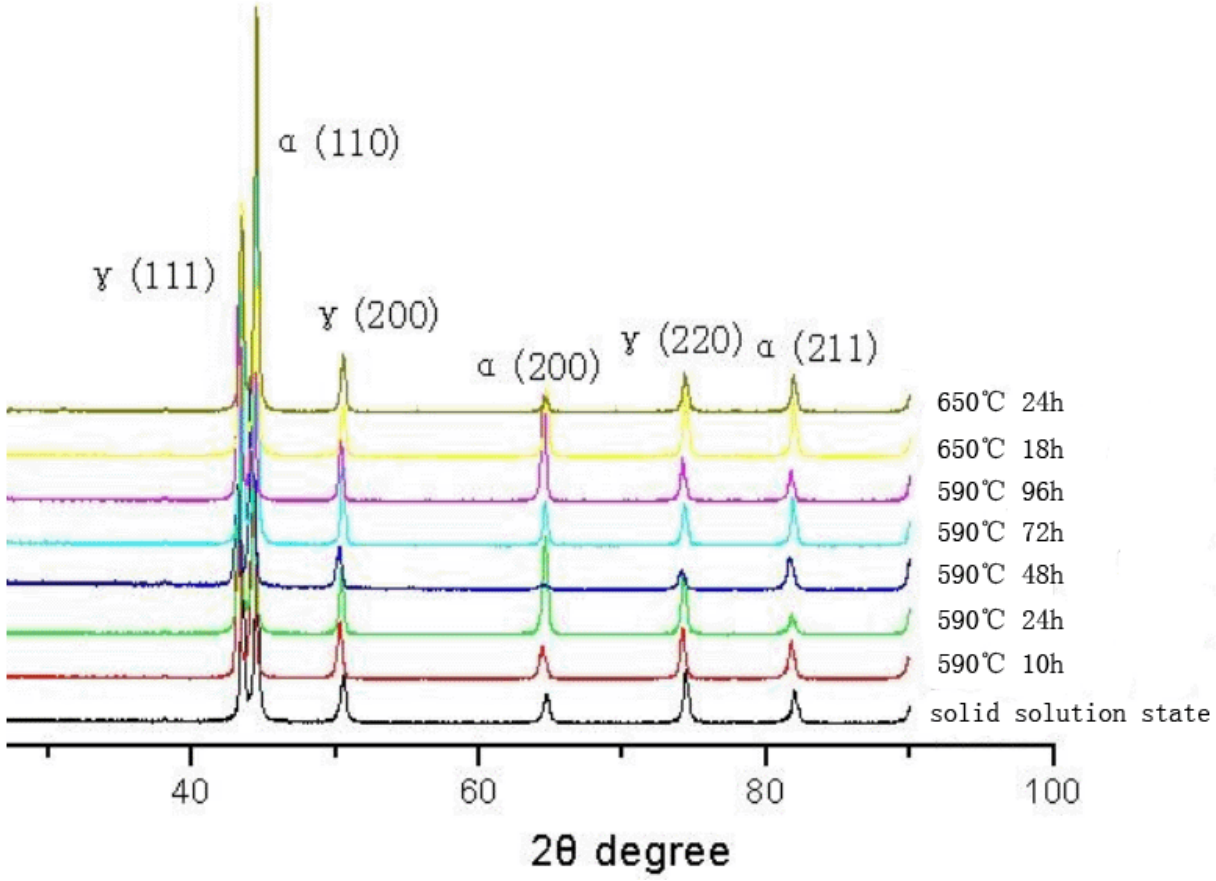

Figure 3. XRD spectra of 2205 DSS after different heat treatment

Fig.3 shows the XRD spectra of 2205 duplex stainless steel aged at different aging temperature for different aging time. In Fig.3, the peaks of the α, γ phase can be indexed in all the samples. However, there is no new phase observed in XRD spectra. This is not consistent with the microstructural results observed by OM. The reason may be that the size of intermediate phases precipitated in the α phase is too small and the amount of that is so little that the XRD apparatus used in current investigation can not detect the signal from the intermediate phases.

3.2. Characterization of the precipitates

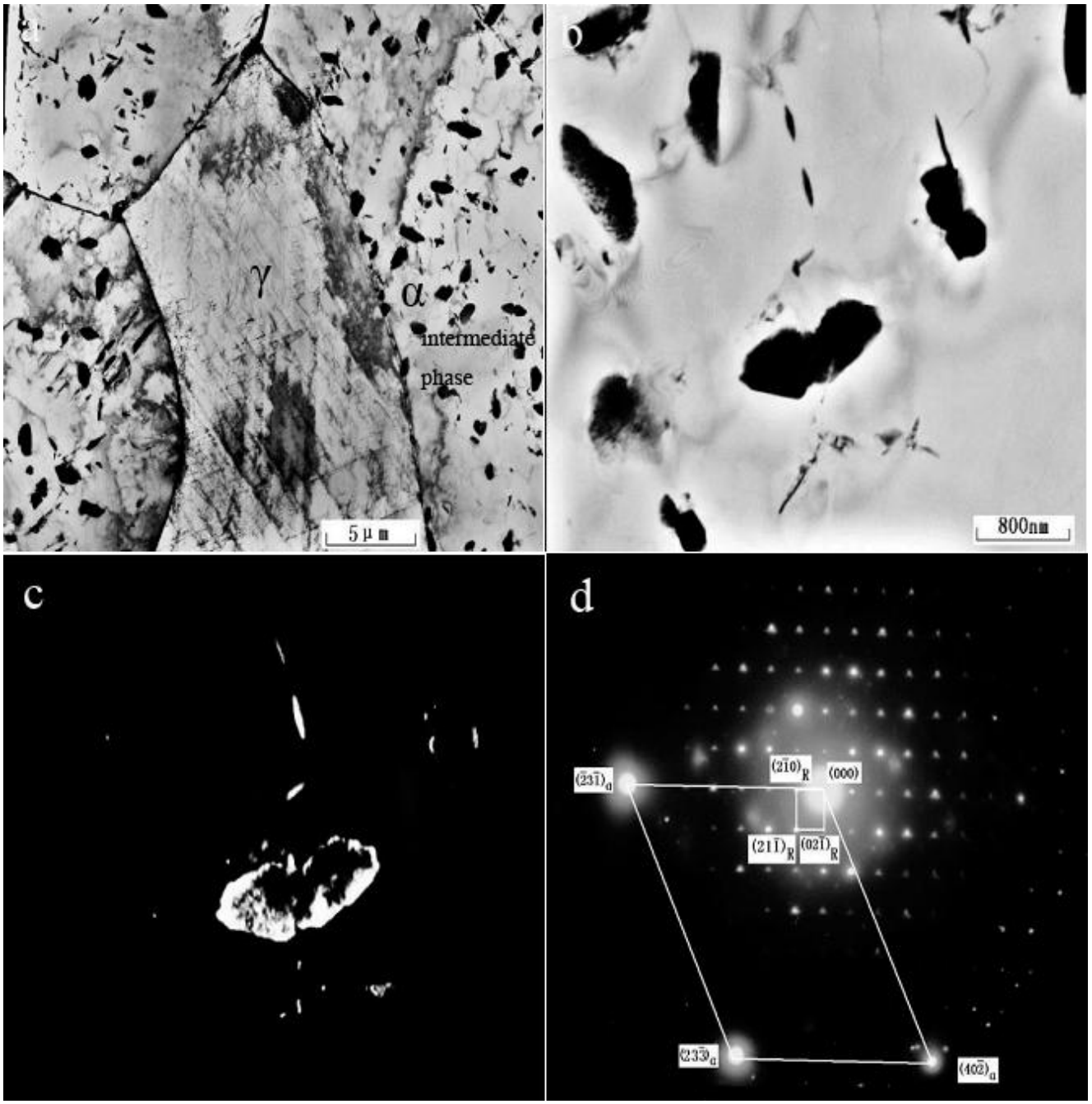

Figure 4. TEM graphs showing the 2205 DSS aged at 590℃ for 96h: (a) the precipitate, (b) bright-field image, (c) dark-field image and (d) the selected area diffraction patterns with the corresponding analysis

Fig.4 shows the TEM micrographs and diffraction patterns of 590℃ for 96h samples. Fig.4(a) indicates that intermediate phase is precipitated from α/γ interface boundary with length in 2~3μm, thickness in 1μm. Figs.4(b) and (c) are bright-field and dark-field images, where as Fig.4(d) shows the selected area diffraction patterns in Figs.4(b) and (c).

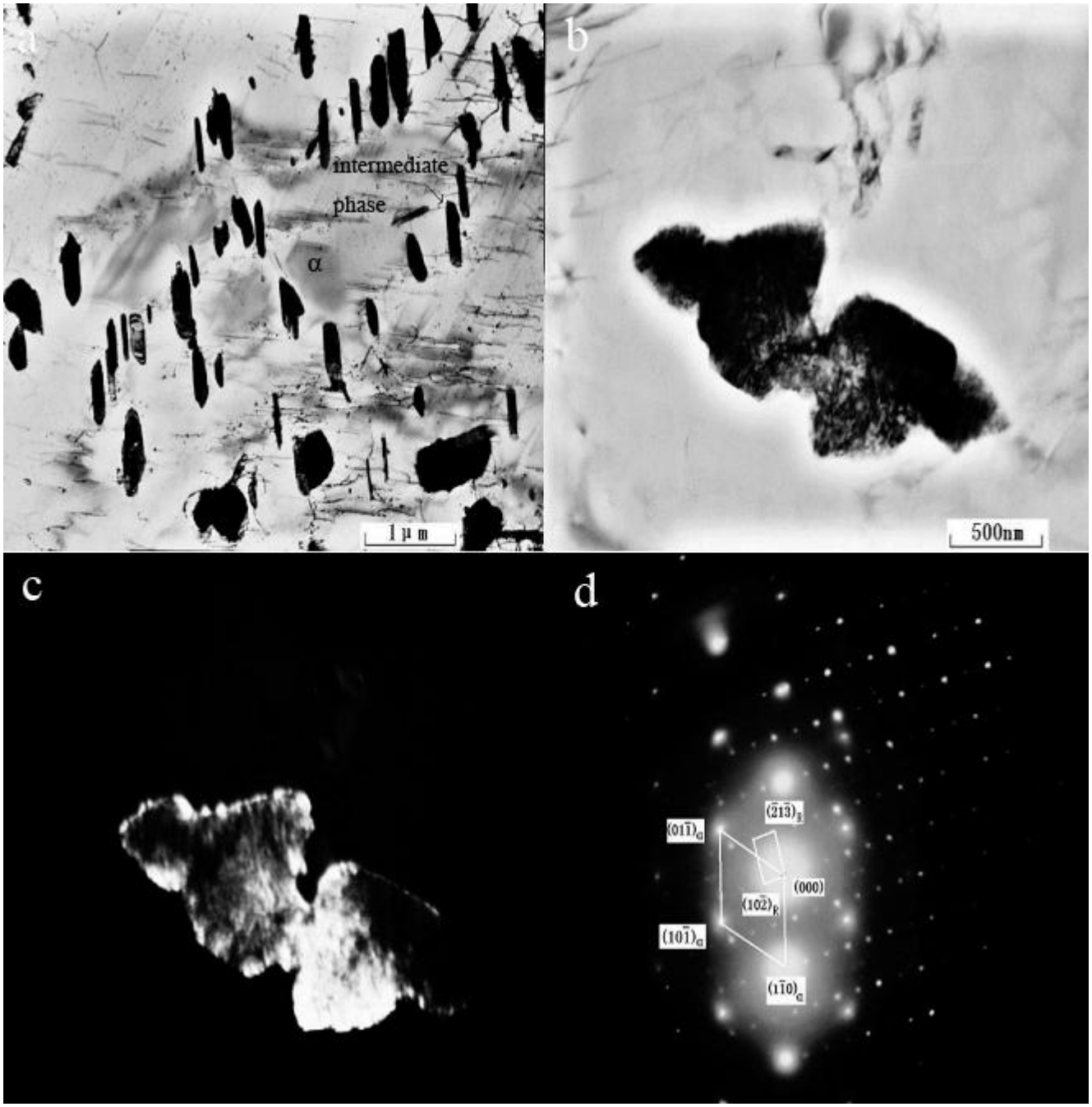

Figure 5. TEM graphs showing the 2205 DSS aged at 650℃ for 18h: (a) the precipitate, (b) bright-field image, (c) dark-field image and (d) the selected area diffraction patterns with the corresponding analysis

In the bright-field and dark-field images, the matrix is α phase. Fig.4(d) reveals that intermediate phase is R phase. Fig.5 and Fig.6 are the TEM micrographs and diffraction patterns of 650℃ for 18h samples. The results suggest that the samples treated at 650℃ for 18h have two intermediate phases, including R phase and σ phase. This is consistent with the results obtained by OM.

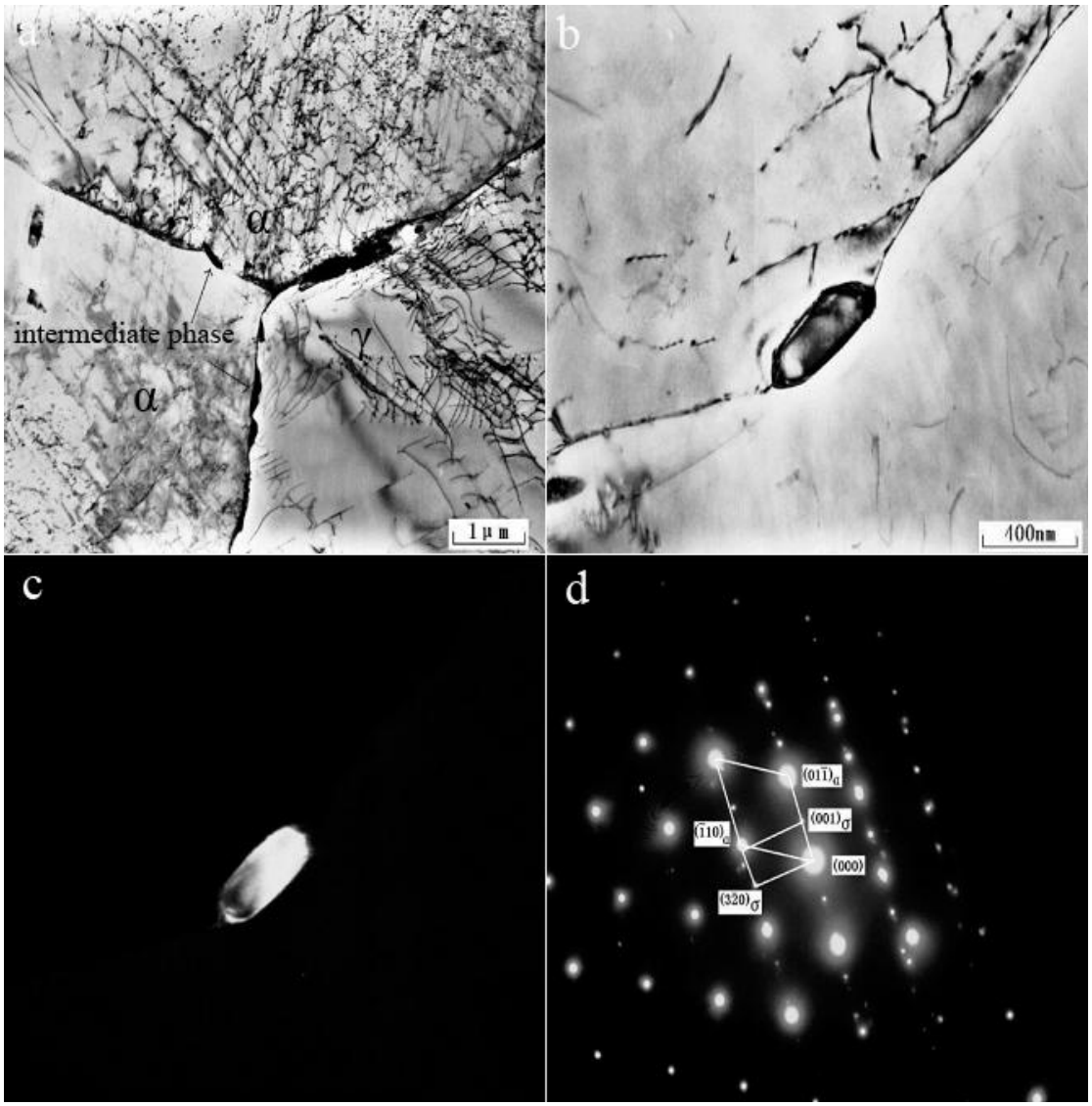

Figure 6. TEM graphs showing the 2205 DSS aged at 650℃ for 18h: (a) the precipitate, (b) bright-field image, (c) dark-field image and (d) the selected area diffraction patterns with the corresponding analysis

3.3. Electrochemical measurements

Fig.7(a) shows the polarization curves of experimental stainless steels aged at 590℃ for different aging time. Meanwhile, the lines with different colours represent different aging time at the same aging temperture 590 ℃(1-10h, 2-24h, 3-48h, 4-72h, 5-96h). The corrosion parameters are summarized in Table 2. According to Fig.7(a) and Table 2, the corrosion potential of the line 5 (around -0.3V) is apparently lower than the other lines. However, the corrosion current increases with the increase of aging time. It means that with the increasing of aging time, the pitting corrosion resistance decreases, which may be related to the amount of the precipitation of the R phase that is rich in the elements of Cr and Mo[11-13]. With the increasing of treating time, more R phases are precipitated in the area so that the amount of Cr and Mo decreases sharply. Nevertheless, Cr and Mo are the main

elements that can improve the corrosion potential in 2205 duplex stainless steel. Therefore, pitting corrosion resistance declines obvious in this area.

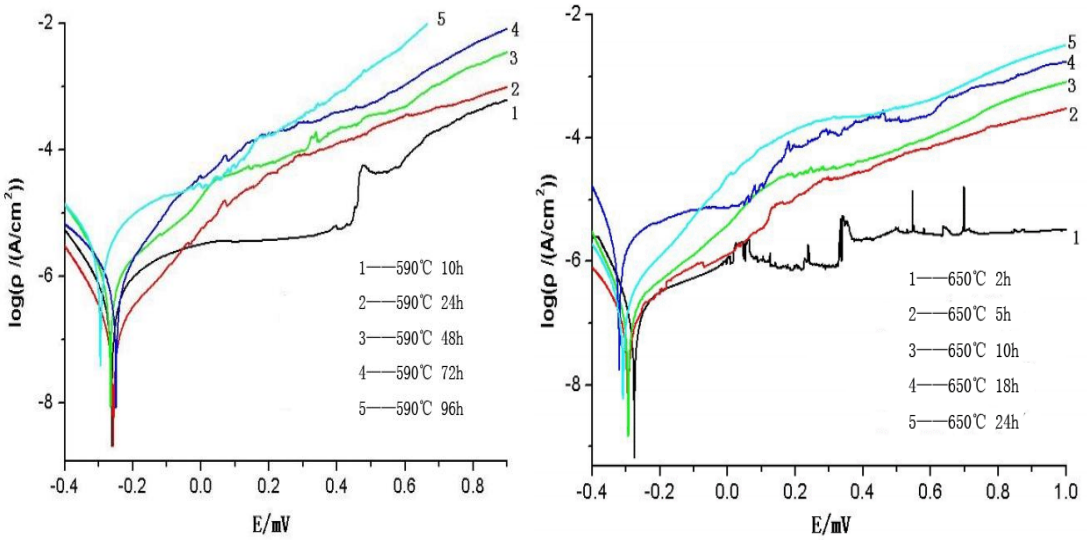

(a) (b)

Figure 7. The polarization curves of 2205 duplex stainless steel aged at different aging temperture for different aging time:(a) 590 ℃ and (b) 650℃.

Table 2 Electrochemical corrosion parameters of 2205 duplex stainless steels aged at different aging temperture for different aging time. E_{corr}: corrosion potential; I_{corr}: corrosion current; b_a: anodic Tafel slope; b_c: cathodic Tafel slope.

Aging Temperature ℃	Aging time h	E_{corr} mV	I_{corr} A/cm^2	b_a mV	b_c mV
590	10	-265	7.589E-8	86	106
	24	-263	1.585E-7	125	104
	48	-271	5.012E-7	112	118
	72	-259	6.309E-7	122	94
	96	-291	3.162E-5	102	119
650	2	-279	2.099E-7	124	114
	5	-284	4.853E-8	122	116
	10	-295	1.114E-7	124	118
	18	-318	1.416E-6	88	136
	24	-310	1.815E-7	121	120

The polarization curves of experimental stainless steels aged at 650℃ for different times are given in Fig.7(b). The corrosion parameters are also summarized in Table 2. As shown in Fig.2(b) and Table 2, different lines indicate different time with the same temperture 650 ℃(1-2h, 2-5h, 3-10h, 4-18h, 5-24h). In Fig.7(b), the corrosion potential of the line 1, 2 (about -0.28V) is higher than that of the line 3 (~-0.3V), 4 (~-0.32V), 5 (~-0.31V). The results show that the pitting corrosion resistance of the

samples aged for 10, 18 and 24h is much worse than that of the samples aged for 2, 5h. Compared with (a), the corrosion potential of the samples processed at 650℃ for 10h is roughly equal to that of the samples processed at 590℃ for 96h. It means that with the increasing of aging temperture, the pitting corrosion resistance decreases more quckly. Combined with TEM images of Figs.4 and 5, it can be analysed that there is not only R phase precipitated,but also σ phase precipitated. Cr and Mo contribute to the pitting corrosion resistance of DSS by providing a protective passive film on the surface[14]. The amount of Cr and Mo reduces in the area where the σ phase is formed, which results in the thinning thickness of the passive film. The pitting may happen more easily in these areas[18-20].

3.4. The corrosion morphology

Fig.8 shows the microstructure of 2205 duplex stainless steel after electrochemical measurement. As is shown in Fig.8(a), the pits mainly distribute in the ferrite phase(α phase). With the aging time increasing, the size of the pits grow up, and the number of the pits also increases. In contrast, the pit in Fig.8(b) is more than that in Fig.8(a). And the pit grow in the ferrite and α/γ interface boundary.

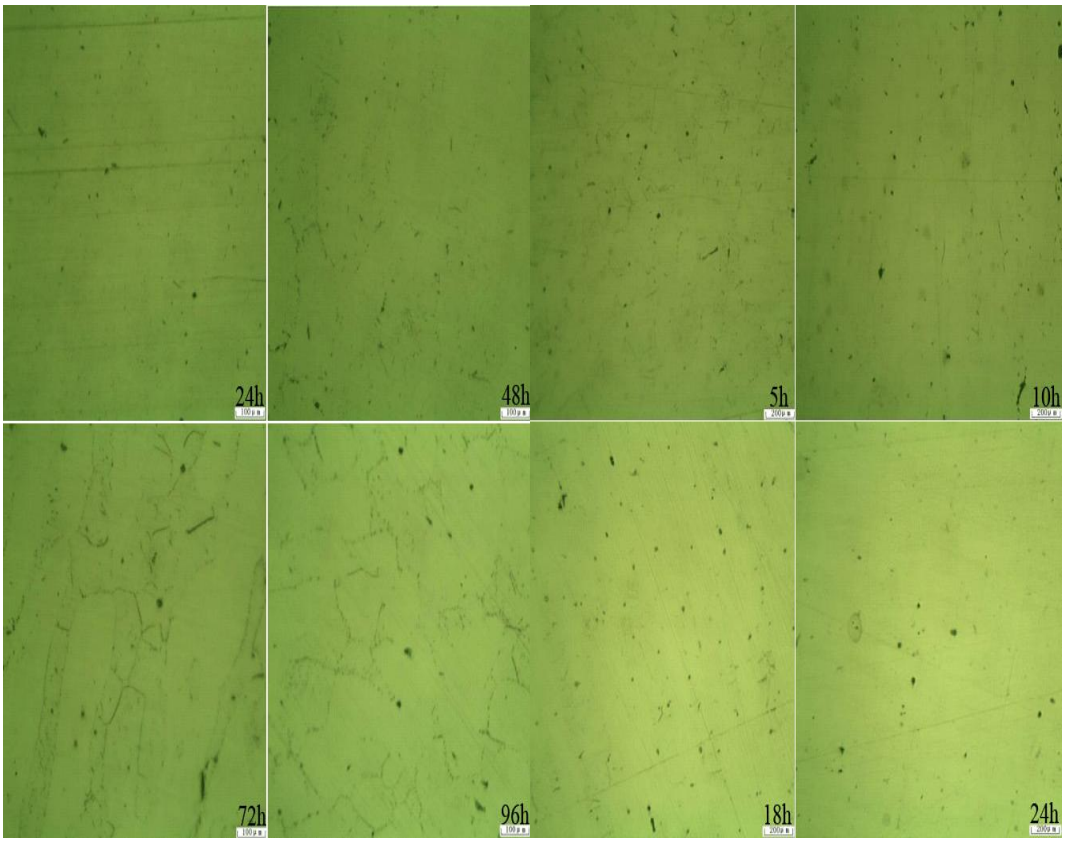

(a) (b)

Figure 8. Morphology of 2205 DSS samples (aged at different temperture: (a) 590 ℃ and (b) 650℃) after electrochemical measurement

Fig.9 shows the SEM images of pits formed on the samples aged at 590 ℃ and 650℃. From Fig.9(a), the pits nucleate in α/γ interface boundary and grow along two phases: α and γ phase. Fig.9(b) reveals the pits nucleate and grow near the intermediate phase which is precipitated from the ferrite phase. The results state that the intermediate phase precipitated during the aging treatment promotes the formed of the pits.

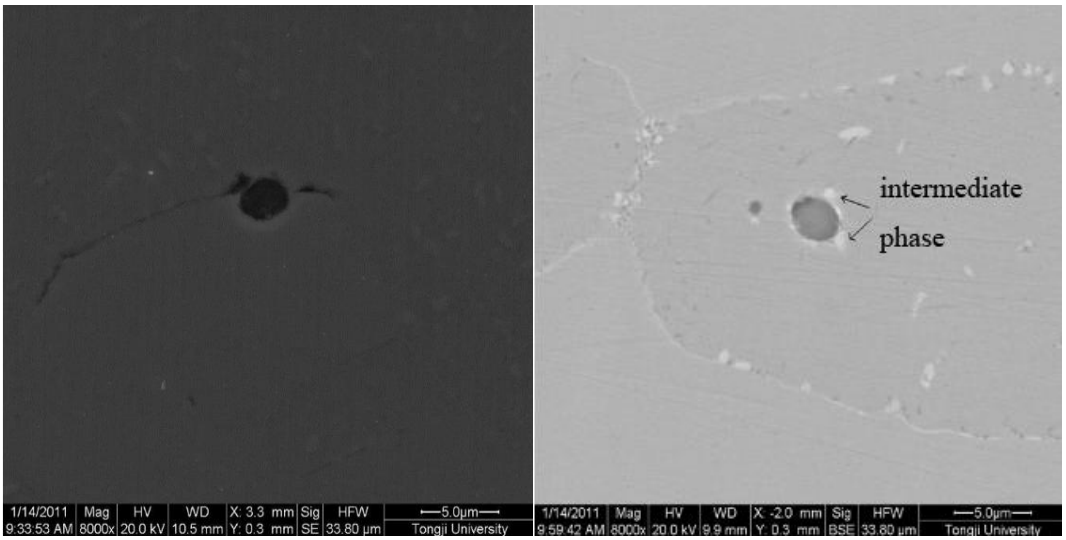

(a) (b)

Figure 9. SEM images of 2205 DSS aged at different temperture after anodic polarization measurement:(a) 590 ℃ and (b) 650℃

4. CONCLUSIONS

(1) 2205 duplex stainless steel has a two-phase structure of α+γ after solid solution treatment; Intermediate phase begins to precipitate after aging 48h at 590 ℃; Intermediate phase begins to precipitate after aging for 5h at 650 ℃; The precipitations concentrate in the α phase and the α/γ phase boundary.

(2) Through TEM phase analysis, the precipitations are found to be R phase at aging temperature of 590℃while R phase and σ phase at aging temperature of 650℃.

(3) The pitting resistance of samples is reduced by aging treatment both at aging temperature of 590℃ and 650℃. The pits tend to nucleate and grow near the precipitations in the ferrite and α/γ phase boundary.

ACKNOWLEDGEMENTS
This work was supported by the ‘Morning Star’ project of the Science and Technological Commission of Shanghai (Grant No 14QA1403600).

References

1. I.N. Bastos, S.S.M. Tavares, F. Dalarda, R.P. Nogueira, *Script. Mater*., 57 (2007) 913–916.

2. B. Deng, Y. Jiang, J. Gong, C. Zhong, J. Gao, J. Li, *Electrochim. Acta*, 53 (2008) 5220–5225.
3. A. Igual Munoz, J. Garcia Anton, J.L. Guinon, V. Perez Herranz, *Corros. Sci.*, 48 (2006) 4127–4151.
4. A.M. do Nascimento, M.C.F. Ierardi, A.Y. Kina, S.S.M. Tavares, *Mater. Charact*., 59 (2008) 1736–1740.
5. Vesna Alar, Ivan Stojanovic, Bruno Zidov3, Franjo Ivusic, *Int. J. Electrochem. Sci.*, 8 **(2013)** 12476 – 12486.
6. S.A. Tavara, M.D. Chapetti, J.L. Otegui, C. Manfredi, *Inter. J. Fatigue*, 23 (2001) 619–626.
7. Hae-Ji Park, Hae-Woo Lee, *Int. J. Electrochem. Sci.*, 9 (2014) 6687 - 6698.
8. Eleonora Bettini, Ulf Kivisakk, Christofer Leygraf, Jinshan Pan, *Int. J. Electrochem. Sci.*, 9 (2014) 61 – 80.
9. K.L. Weng, H.R. Chen, J.R. Yang, *Mater. Sci. Eng.* A, 379 (2004) 119-132.
10. H M. Ezuber, A. El-Houdb, F. El-Shawesh, *Desalination* 207 (2007) 268–275.
11. A. RedjaÏmia, J. P. Morniroli, P. Donnadieu, G. Metauer, *Mater. Sci*. 37(2002)4079-4091.
12. Yukio Shimoide, Jie Cui, Chang-Yong Kang, Kazuya Miyahara, *ISIJ International*, 39 (1999)191-194.
13. Jie Cui, In-Sung Park, Chang-Yong Kang, Kazuya Miyahara, *ISIJ International*, 41 (2001)192-195.
14. K.N. Adhe, V. Kain, K. Madangopal, H.S. Gadiyar, *JMEPEG*, 5 (1996) 500-506.
15. J.O. Nilsson, *Mater. Sci. Technol*., 8 (1992) 685-700.
16. K. Ravindranath and S.N. Malhotra, *Corros. Sci.*, 137 (1994) 121-132.
17. T.M. Devine, *J. Electrochem. Soc*., 126 (1979) 374-385.
18. J.K.L. Lai, K.W. Wong , D.J. Li. *Materials Science and Engineering A*, 203 (1995) 356-364.
19. F. Elshawesh, N. Elahresh, A. Elhoud. *Br. Corros. J*., 33 (1998) 285-287.
20. N. Lopez,M. Cid,M. Puiggali. *Corros. Sci*., 41 (1999) 1615-1631.